




# Comprehensive in silico analyses of keratin heterodimerisation

Nicole Schwarz<sup>a</sup>, Rudolf E. Leube<sup>a</sup>, Stefan Düsterhöft<sup>b,\*</sup> 

<sup>a</sup> Institute of Molecular and Cellular Anatomy, RWTH Aachen University, Wendlingweg 2, Aachen 52074, Germany

<sup>b</sup> Institute of Molecular Pharmacology, Medical Faculty, RWTH Aachen University, Wendlingweg 2, Aachen 52074, Germany

## ARTICLE INFO

### Keywords:

Keratin  
Intermediate filaments  
Keratin heterodimerisation  
AlphaFold multimer

## ABSTRACT

Keratins are the largest and most diverse group of intermediate filament proteins, providing structural integrity and mechanical strength to epithelial cells. Although their assembly as heterodimers is well established, the specific pairing preferences and molecular basis of keratin dimerisation remain largely unknown. Here, we employ a high-throughput computational pipeline that integrates AlphaFold Multimer (AFM) modelling, VoroIF-GNN interaction interface quality assessment, interaction energy calculations and structural comparisons with experimentally solved structures to systematically investigate keratin heterodimerisation and to provide a guideline for further analysis of intermediate filament assembly. To validate our in silico approach, we include the well-studied vimentin homodimer as a reference. The predicted vimentin homodimer shows strong agreement with available experimental data, supporting the accuracy of our modelling pipeline. Our results show that keratin heterodimers generally have lower interaction energies, indicating more favourable interactions, than their homodimer counterparts, and exhibit structural configurations that closely resemble known intermediate filament structures. Comparative analyses of different keratin pairs also reveal the importance of the coil 1 region for dimer stability. Furthermore, co-expression of keratin pairings is demonstrated by analysis of spatial transcriptomics data in skin under physiological and pathological conditions. Collectively, these findings highlight structural principles underlying canonical keratin heterodimerisation and establish a robust computational workflow for elucidating alternative keratin dimerisations.

## 1. Introduction

Intermediate filaments (IFs) are essential cytoskeletal components that provide mechanical stability and elasticity to cells. IFs share a common tripartite structure with an alpha-helical rod domain that is flanked by intrinsically disordered head and tail domains. Keratins represent the largest subset of IFs. They are prominently expressed in epithelia and their associated structures such as hair and nails. Each keratin polypeptide shows a unique distribution pattern (Moll et al., 2008). Based on sequence homology, keratins are divided into the type I (acidic) and type II (basic to neutral) polypeptides, which form obligate heterodimers with a precise 1:1 stoichiometry. In vitro analyses revealed a high degree of promiscuity in pair formation (Hatzfeld and Franke, 1985). These heterodimers associate to form higher order polymers that build up the mature ~10 nm intermediate filaments (Schwarz and Leube, 2023; Yoon and Leube, 2019).

Keratins are involved in a wide range of cellular processes, strengthening cells against mechanical damage, modulating signalling

pathways and regulating proliferation, differentiation and apoptosis (Redmond and Coulombe, 2021). For example, in the epidermis the proliferating basal-layer keratinocytes express the keratin 5 (type II) and keratin 14 (type I) pair (Cohen et al., 2022). In contrast, the differentiating suprabasal keratinocytes produce keratins 1 and 10 (Cohen et al., 2022). In certain body regions, in situations of hyperproliferation and after wounding additional keratin pairs occur. Thus, keratins 6a-c, 16 and 17 are produced in palmoplantar skin, during wound repair and in disease conditions such as inflammation and carcinogenesis (Cohen et al., 2024; Wiedemann et al., 2023). Moreover, single point keratin gene mutations give rise to a large number of autosomal dominant skin diseases with multiple phenotypes, which reflect the localization and function of the affected keratin polypeptide (Toivola et al., 2015).

Although considerable knowledge has been gained about canonical IF pairings, the understanding of alternative pairings remains incomplete. These include non-canonical keratin heterodimers or even keratin homodimers. Key questions arise: Why are certain pairings preferred? Are canonical pairings also biochemically most favoured? Could

\* Corresponding author.

E-mail address: [sduesterhoeft@ukaachen.de](mailto:sduesterhoeft@ukaachen.de) (S. Düsterhöft).

<https://doi.org/10.1016/j.ejcb.2025.151513>

Received 1 April 2025; Received in revised form 1 July 2025; Accepted 27 August 2025

Available online 29 August 2025

0171-9335/© 2025 The Author(s).

Published by Elsevier GmbH. This is an open access article under the CC BY license

(<http://creativecommons.org/licenses/by/4.0/>).

alternative pairings be relevant for epithelial adaptation and homeostasis? Addressing these questions comprehensively by experimental in vitro testing is prohibitively expensive and time-consuming.

Furthermore, despite extensive biochemical and genetic studies, the structural determinants that govern dimer specificity are still not fully understood. Traditional experimental structure determination techniques, such as electron microscopy and X-ray crystallography, have provided valuable insights into the coiled-coil nature of keratin rod domains. However, these approaches are severely limited by the complexity of full-length keratin heteropolymers and their propensity to aggregate. Consequently, to date, only partial coiled-coil structures have been resolved experimentally for the keratin pairs KRT1-KRT10 and KRT5-KRT14 (Bunick and Milstone, 2017; Eldirany et al., 2019; Lee et al., 2012, 2020; Lomakin et al., 2020). In contrast, the type III IF vimentin homodimer has yielded more extensive - although still incomplete - experimentally resolved structures, making the vimentin homodimer a valuable structural reference (Aziz et al., 2012; Nicolet et al., 2010; Pang et al., 2018; Strelkov et al., 2002).

A high-throughput approach is essential to overcome the challenges of in vitro analysis to explore canonical and alternative dimer pairings. Taking advantage of AlphaFold Multimer (Evans et al., 2021; Jumper et al., 2021; Mirdita et al., 2022) we have developed a high-throughput computational pipeline for modelling and analysing keratin dimers. Importantly, a recent comprehensive study has demonstrated that AlphaFold2 can predict coiled-coil structures with unprecedented accuracy (Madaj et al., 2025). By focusing on the coiled-coil rod domain that is crucial for dimerisation of IFs, our approach bypasses the challenges posed by the intrinsically disordered head and tail domains.

In this study, we used vimentin homodimer models as a control to validate the predictive accuracy of AlphaFold Multimer and our subsequent energy-based refinement and analysis. By comparing the interaction interfaces of keratin dimers, we identified putative alternative dimer pairings. In addition, we analysed data from spatial transcriptomics datasets to investigate the co-expression of keratin pairings in epidermal cells under both physiological and pathological conditions.

This comprehensive predictive overview provides a robust framework for generating new hypotheses about IF dimer formation, paving the way for more targeted and efficient in vitro assays. In conclusion, our study not only advances the understanding of known keratin dimerisation, but also lays the groundwork for the exploration of non-canonical pairings, providing valuable insights into the structural and functional diversity of keratin filaments. Furthermore, our study provides a robust guideline to approach and study the IF space with in silico techniques.

## 2. Material and methods

### 2.1. Structural modelling of intermediate filament dimers

Sequences of type I and type II keratins and control proteins were obtained from the UniProt database (UniProt, 2024).

Type II keratins: KRT1 (P04264), KRT2 (P35908), KRT3 (P12035), KRT4 (P19013), KRT5 (P13647), KRT6A (P02538), KRT6B (P04259), KRT6C (P48668), KRT7 (P08729), KRT8 (P05787), KRT71 (Q35Y84), KRT72 (Q14CN4), KRT73 (Q86Y46), KRT74 (Q7R7S7), KRT75 (Q95678), KRT76 (Q01546), KRT77 (Q7Z794), KRT78 (Q8N1N4), KRT79 (Q5XKE5), KRT80 (Q6KB66), KRT81 (Q14533), KRT82 (Q9NSB4), KRT83 (P78385), KRT84 (Q9NSB2), KRT85 (P78386), KRT86 (Q43790)

Type I keratins: KRT9 (P35527), KRT10 (P13645), KRT12 (Q99456), KRT13P13646, KRT14 (P02533), KRT15 (P19012), KRT16 (P08779), KRT17 (Q04695), KRT18 (P05783), KRT19 (P08727), KRT20 (P35900), KRT23 (Q9C075), KRT24 (Q2M2I5), KRT25 (Q7Z3Z0), KRT26 (Q7Z3Y9), KRT27 (Q7Z3Y8), KRT28 (Q7Z3Y7), KRT31 (Q15323), KRT32 (Q14532), KRT33A (O76009), KRT33B (Q14525), KRT34 (O76011), KRT35 (Q92764), KRT36 (O76013), KRT37 (O76014), KRT38 (O76015), KRT39 (Q6A163), KRT40 (Q6A162).

Other proteins: DES (P17661), VIM (P08670), NEFL (P07196), NES (P48681), LMNA (P02545), LMNB1 (P20700), LMNB2 (Q03252), BFPSP2 (Q13515), GAPDH (P04406), ACTB (P60709), HMBS (P08397).

Full amino acid sequences were retrieved using the UniProt API (UniProt, 2024) through a custom Python script (Python v3.11.0) using the requests (v2.32.3) and pandas (v2.1.4) libraries. Structural data for monomeric proteins were obtained from the AlphaFold2 protein structure database (Jumper et al., 2021; Varadi et al., 2022). Confidence scores (pLDDT, predicted local distance difference test) were extracted from the downloaded PDB files. For high-throughput dimer modelling, protein sequences were truncated to focus on the structural regions of IFs by removing disordered head and tail regions while retaining high confidence segments. Custom Python scripts using the pandas (v2.1.4) and numpy (v1.24.3) libraries managed the sequence data and implemented truncation logic. Regions with pLDDT scores greater than 90 were identified as high-confidence structural regions. We extended each of these identified highly structured core segments by up to 20 residues on both sides to include flanking regions with intermediate pLDDT scores (80–90). This ensures more consistent input lengths of coiled-coil segments for modelling with AlphaFold Multimer and preserves boundary context that may still be relevant for keratin dimer formation.

*Ab initio* structure prediction of IF dimers was performed using the deep learning algorithm AlphaFold Multimer (AFM) (Jumper et al., 2021) in a high-throughput batch pipeline based on the ColabFold notebook v1.5.5 (Mirdita et al., 2022). Structural modelling with AlphaFold Multimer was performed without homology templates, using MMseq2 for multiple sequence alignment. Each protein pair was modelled in two iterations per structure, generating 10 dimer complexes per pair. The models were ranked according to the multimer score ipTM (interface predicted template model) and the best-ranked models were used for subsequent analysis. Other filament and non-filament proteins were included as controls. ChimeraX (v1.7.1) was used to visualise the structures (Pettersen et al., 2021).

The ipTM scores, which represent the confidence in the predicted interaction interfaces between protein pairs in the dimers, were visualised using a heatmap generated by a custom Python code. The heatmap was constructed using matplotlib (v3.9.2), with the scores represented by a colour map and proportional rectangle sizes. ipTM scores of less than 0.50 indicate poor interface prediction, while scores of 0.50–0.70 indicate moderate confidence, and scores greater than 0.70 indicate high confidence.

### 2.2. Structural alignment and root-mean-square deviation (RMSD) calculation

The predicted AFM models of the dimers were aligned using the MatchMaker function in ChimeraX (v1.7.1) (Pettersen et al., 2021). Structural agreement between predicted and experimental coordinates was quantified using RMSD (root-mean-square deviation) of C $\alpha$ -atoms. Values below 2 Å denote very good, near-atomic agreement, 2–4 Å indicate good to moderate structural similarity, and values above ~4 Å reflect poor or incorrect matches. RMSD values between aligned protein structures were calculated with a custom Python script, using the Bio.PDB module of Biopython (v1.84) for PDB parsing and residue mapping, and the numpy library (v1.24.3) for numerical calculations.

### 2.3. Analysing interaction energies of predicted dimers

The FoldX5 force field (Van Durme et al., 2011) was employed for structural model refinement of predicted dimers and analysis. Ten consecutive rounds of side-chain structural relaxation were performed to minimise the energy of the dimer models. After refinement, FoldX5 was used to calculate interaction energies, identify interfacial residues and detect backbone collisions, which indicate poor model quality in the relaxed models. FoldX5 applies electrostatic screening using a generic ionic-strength parameter (rather than explicit salt species). Energy

calculations were performed at ionic strengths of 50, 150 and 300 mM. The interaction energies calculated at 150 mM, which is the approximate physiological salt condition, were visualised using a heatmap generated with custom Python code. The heatmap was constructed using matplotlib (version 3.9.2), with the results represented by a colour map and inversely proportional rectangle sizes. FoldX5 was also used to calculate effect of single point mutations on dimer stability and interaction energy.

Furthermore, the quality of the predicted interaction interface of all relaxed dimer models was assessed using VoroIF-GNN (Voronoi Inter-Face Graph Neural Network), a Voronoi tessellation-derived protein–protein interface assessment tool (Olechnovic and Venclovas, 2023). The weighted average pCAD (predicted Contact Area Difference) score was used for comparison, with scores close to 1 representing high-quality interfaces and scores close to 0 representing low-quality interfaces.

#### 2.4. Analysis of keratin expression in skin using single cell and spatial transcriptomics

Curated and processed spatial transcriptomics datasets from STOmicsDB (Xu et al., 2024) were utilised to analyse the expression levels of keratins in skin under both physiological and pathological conditions. The analysis encompassed datasets from healthy controls as well as from patients with atopic dermatitis (GSE197023) and cutaneous squamous cell carcinoma (GSE144239) (Ji et al., 2020).

Custom Python scripts were used to process, analyse and visualise these data. The processing pipeline read.h5ad files and mapped keratin gene identifiers using the built-in modules os and glob (Python v3.11.0), together with pandas (2.1.4), scanpy (v1.11.0) and mygene (v3.2.2). Gene expression levels were calculated and visualised using numpy (v1.21.2), scipy.stats (v1.13.1) and matplotlib (v3.9.2). For visualisation, bubble heatmaps were generated.

### 3. Results

#### 3.1. Using vimentin homodimer to validate computational prediction of intermediate filament polypeptide dimerisation

To evaluate the predictive power of AlphaFold Multimer (AFM) for IF polypeptide dimerisation, we modelled the full-length vimentin homodimer whose structure has been partially solved experimentally (Fig. 1A). In the best AFM model out of five a high level of structural confidence and model quality was noted for coil 2, as indicated by the high predicted local distance difference test (pLDDT) values between 80 and 100. In contrast, coil 1 exhibited only low to moderate pLDDT values between 50 and 80, with coil 1 A also failing to form a proper dimer structure. In addition, the head (N-terminus) and tail (C-terminus) regions showed low pLDDT values below 30, consistent with their known intrinsic disorder and flexibility (Zhou et al., 2021). While the modelling of coil 2 and the disordered head and tail regions were consistent with the expected structure, the poor prediction quality of coil 1 led us to conclude that the full-length vimentin model was insufficient for detailed structural analysis. Furthermore, the overall structure model only has an ipTM score of 0.34, indicating a very poor modelling confidence of the dimer interaction.

To improve predictive power, model quality and computational efficiency, we split vimentin into separate coil 1 and coil 2 regions, removing the unstructured N- and C-termini. This refinement significantly improved the modelling of coil 1, as evidenced by much higher pLDDT scores and the complete formation of the coil 1 dimer (Fig. 1B). The refined model achieved an overall moderate ipTM (interface predicted template modelling) score of 0.5 (coil 1) and 0.56 (coil 2), an additional metric assessing the quality of the predicted protein–protein interaction (Fig. S1A). Importantly, although ipTM scores fell into the moderate range, our predicted vimentin homodimer models retained

high pLDDT values and closely matched experimentally determined Protein Data Bank (PDB) structures for both coiled-coil regions of the vimentin homodimer (Fig. 1C, Fig. S2A), which supports the validity of the models and approach. The differences between the predicted and experimental structures were minimal. Most residues deviated only by an RMSD of 0–2 Å, which is consistent with very good near-atomic agreement, while a smaller subset of residues were shifted moderately by an RMSD of 3–4 Å. Only a handful of residues exceeded 4 Å, and these all occur at the truncated termini of the experimentally solved structures. For comparison, the experimental structures have a resolution of 1.8–2.8 Å, meaning that the predictions are highly consistent with the level of detail seen in the experimental data. This strong agreement highlights the accuracy of the modelling approach.

Overall, the results demonstrated that focusing on individual coiled-coil regions enhances model reliability, thus allowing for more accurate predictions of IF dimer formation. Remarkably, segmenting coiled-coil domains and excluding disordered head and tail regions mirrors the fragment-based strategies used in the experimental determination of IF structures (Chernyatina et al., 2016; Strelkov et al., 2001). This strategy helped to overcome and deal with the unique properties of IFs, such as their conformational variability, poor solubility and strong tendency to assemble into higher-order filament polymers.

#### 3.2. High throughput computational analysis shows differences in dimer formation of intermediate filament polypeptides

Having validated our approach for predicting vimentin homodimer structures, we extended it to a high-throughput analysis of keratin combinations and other intermediate filament polypeptides including the cytoplasmic neurofilament polypeptide L, nestin and desmin as well as nuclear lamins. Control proteins were GAPDH,  $\beta$ -actin and HMBS. Importantly, the GAPDH dimer was correctly identified with very high interaction confidence, as reflected by a high ipTM score of 0.95 (Fig. S1A). Conversely, HMBS showed a very low ipTM score of 0.26, accurately indicating no homodimerisation (Fig. S1A). Similarly,  $\beta$ -actin also had a very low ipTM value of 0.28 for homodimerisation, indicating the absence of a predicted interaction (Fig. S1A). The  $\beta$ -actin result highlights a known limitation of AlphaFold2. It does not account for the binding of additional biomolecules or post-translational modifications. As actin polymerisation is driven by bound ATP, AlphaFold2 is unable to model this interaction.

Overall, the predictions for the control protein homodimers agreed well with the expected results. In addition, as expected, GAPDH and HMBS showed no predicted interaction or heterodimer formation with IF proteins (Fig. S1A). Interestingly, high confidence heterodimers (indicated by higher ipTM scores in a range between 0.6 and 0.85) were predicted between  $\beta$ -actin and the coil 2 regions of many keratins and vimentin, but not between  $\beta$ -actin and coil 1 (ipTM scores below 0.3). This finding suggests specific interaction preferences of IF polypeptide subdomains. It is remarkable considering reports showing coordination of actin filaments and keratin filaments, especially small keratin filament precursors (Kölsch et al., 2009). It has been assumed that this is due to cross-linkers, most notably plectin (Outla et al., 2025). The current data offer the possibility that direct interactions occur between actin and keratins. This is also supported by observations for vimentin (Wu et al., 2022).

All models of keratin coil 1 and coil 2 exhibited high local structural confidence. Most per-residue pLDDT values were consistently above 75 in the structured coiled-coil regions, while those in the expected flexible linker regions fell below 50. The ipTM values for canonical filament heterodimer models indicated moderate confidence, ranging from 0.5 to 0.6 (Fig. S1A) similar to the range of the vimentin homodimers. Notably, the noncanonical keratin homodimers, particularly for coil 1, exhibited lower ipTM values below 0.5 and occasional backbone clashes in the predicted models, indicating lower model quality. These results suggest that keratin heterodimers are favoured over homodimers by AlphaFold2

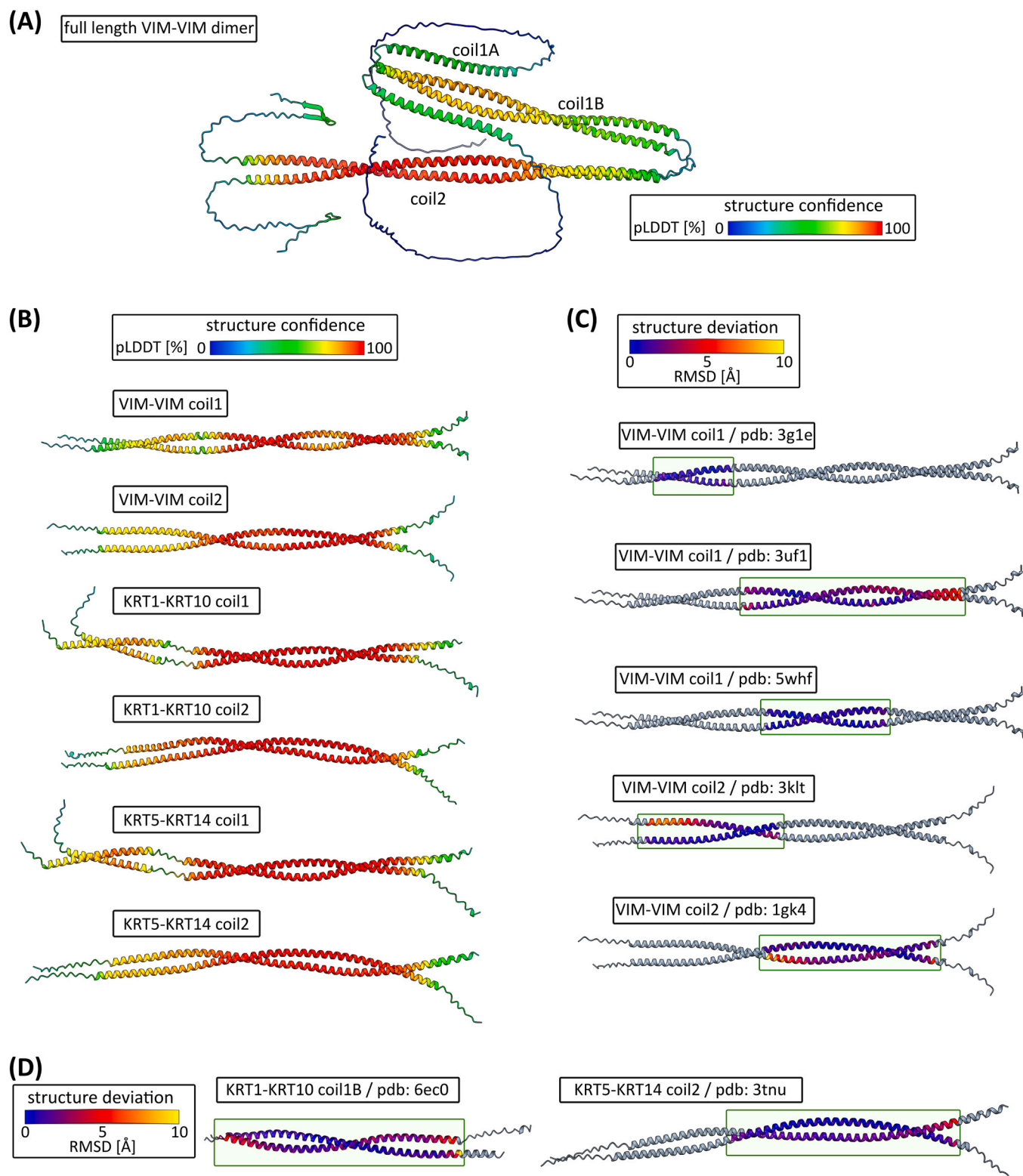


**Fig. 1.** Structural models of IF polypeptide dimers. All structures are shown as cartoon representations. (A) The best-ranked alpha-fold multimer (AFM) model of the full-length vimentin (Vim) homodimer, coloured by pLDDT (predicted local distance difference test, [%]) scores. (B) The best-ranked AFM models of the coil 1 and coil 2 regions of the indicated dimers, coloured by pLDDT scores. (C-D) Comparison of the best-ranked AFM models of coil 1 and coil 2 regions of the indicated dimers of vimentin (C) as well as KRT1-KRT10 and KRT5-KRT14 (D) with experimentally solved structures (PDB IDs shown). Models are coloured according to the calculated RMSD values from the structure comparisons (good agreement, RMSD = 0 Å: blue; poor agreement, RMSD  $\geq$  4 Å: red to yellow). Corresponding superpositions/alignments are shown in Fig. S2A,B.



prediction.

Importantly, while the ipTM scores for the predicted heterodimers were moderate, structural comparisons with experimentally resolved structures again showed high concordance. Both the KRT1-KRT10 coil 1 heterodimer and the KRT5-KRT14 coil 2 heterodimer showed strong structural agreement with their respective experimentally resolved structures (Fig. 1D, Fig. S2B). As before, the differences between the predicted and experimental structures were minimal, with most RMSD values falling within the range of 0–2 Å. A few values were between 3 and 4 Å, and only very few exceeded 4 Å at the periphery of the truncated termini of the experimentally solved structures. More generally, all IF dimer models predicted by AFM consistently showed high structural similarity to the experimentally determined IF structures (Fig. 1B–D). These results highlight the reliability of AFM predicted models for further analysis.

To complement the AFM ipTM confidence score, we used the VoroIF-GNN (Voronoi InterFace Graph Neural Network) machine learning model (Olechnovic and Venclovsky, 2023) to evaluate the interaction interfaces of the predicted dimer structures (Fig. S1B). Overall, the VoroIF score showed a very similar pattern when compared with the ipTM scores (Fig. S1A,B). Notably, the analysed keratin heterodimer models and the vimentin homodimer model showed an overall very high interface quality (KRTs: 0.9–1.0; VIM: 0.85). This provided further support for the accuracy of the predicted models.

To gain further insight into the keratin pairings, interaction energies of coil 1, coil 2 and both together (total) were calculated using the FoldX force field (Fig. 2A, B, Table S1). Directly compared to the vimentin homodimer (vimentin homodimer set to  $\Delta\Delta G = 0$  kcal/mol), canonical keratin type I-type II heterodimers were energetically favoured, as reflected by their lower interaction energies ( $\Delta\Delta G$  between  $-10$  kcal/mol up to  $-50$  kcal/mol for either coil 1 or coil 2), indicating stronger interactions. In contrast, keratin homodimers exhibited much higher interaction energies ( $\Delta\Delta G$  between  $+10$  kcal/mol up to  $+50$  kcal/mol for either coil 1 or coil 2), confirming that they are less stable and less energetically favoured than heterodimers (Fig. 2A, B). Furthermore,

non-canonical type I-type I and type II-type II heterodimers also showed high interaction energies compared to canonical type I-type II heterodimers (Fig. 2A, B). Thus, canonical type I-type II heterodimers are energetically most favourable.

Notably, our modelling and evaluation showed that vimentin-type I keratin heterodimers seem to be more favourable than vimentin homodimers. This is consistent with earlier reports of VIM-KRT14 dimer formation (Kuburich et al., 2024; Steinert et al., 1993; Velez-delValle et al., 2016).

In addition, IF polypeptide dimers, characterised by their larger interfaces, generally exhibited higher interaction energies than the GAPDH dimer control (Fig. 2A). Interestingly, lamin dimers have the lowest interaction energies ( $\Delta\Delta G$  around  $-50$  kcal/mol) compared to the vimentin homodimer, mainly driven by coil 1 (Fig. 2A, B).

Taken together, these results highlight the preference for type I-type II heterodimer formation in keratins and the robustness of the AFM pipeline to capture biologically meaningful IF structures.

### 3.3. Interaction energy analysis reveals preferred pairings of canonical and non-canonical keratin heterodimers

Since the AlphaFold2 confidence metrics show only moderate differences between type I-type II heterodimers (with ipTM values between 0.5 and 0.6; Fig. 3A), we wanted to gain deeper molecular insights based on the predicted structures themselves. Therefore, we again assessed the quality of the interaction interface of all type I-type II heterodimers using VoroIF-GNN. All possible canonical and non-canonical type I-type II heterodimers showed high quality interfaces with VoroIF scores between 0.8 and 1.0 (Fig. S3A). Additionally, we calculated and compared the interaction energies using the FoldX force field for models of all heterodimers (Fig. 3A, Fig. S3B, Table S1). These calculations yielded a wide range of interaction energies for different pairings, with differences between pairings up to 70 kcal/mol for coil 1 and coil 2 individually, and up to 80 kcal/mol when considering the total interaction energy (Fig. 3A, Fig. S3B).

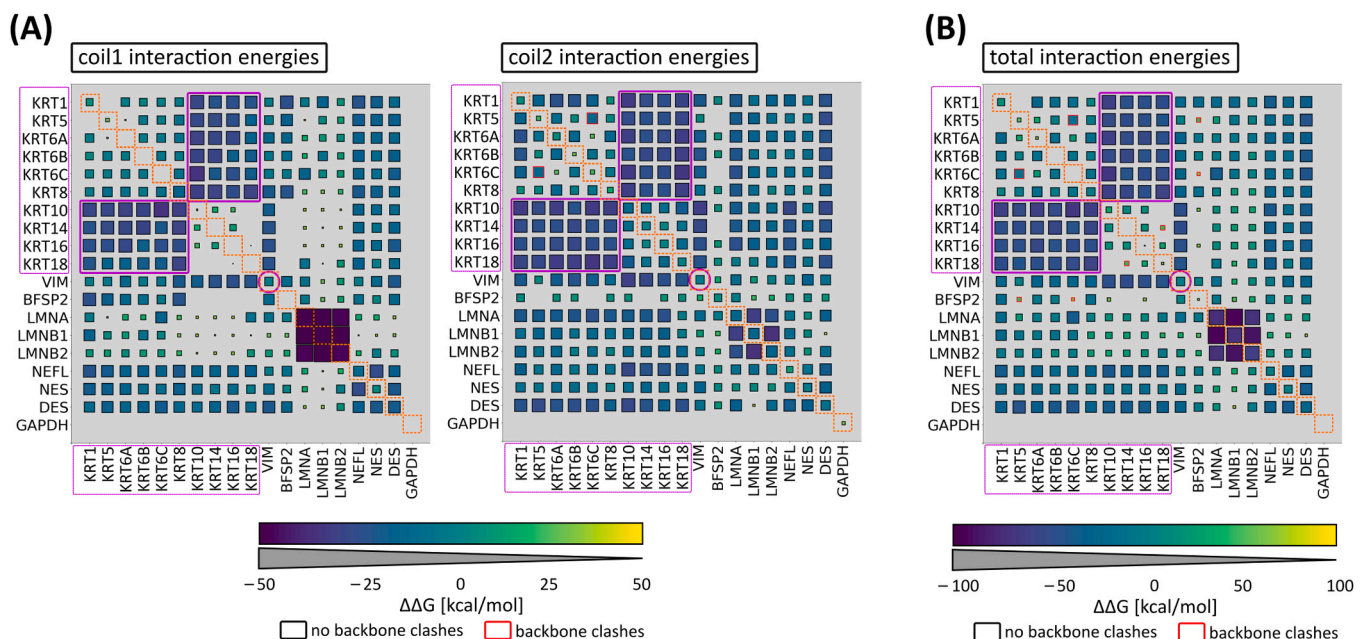


**Fig. 2.** Overview of interaction energies of intermediate filament polypeptide dimers. All interactions energies are compared to that of the vimentin homodimer. (A–B) Heatmaps show the interaction energies for the relaxed, best-ranked dimer predictions of coil 1 and coil 2 as well as both combined (total) at 150 mM ionic strength. Smaller boxes represent higher interaction energies (less favourable interactions), while larger boxes correspond to lower energies (more favourable interactions). Red borders around value boxes indicate backbone collisions, indicating poor quality prediction models. Interaction energies are normalised to the vimentin homodimer, whose energy is set to 0, for (A) coil 1 and coil 2 as well as (B) both combined (total). Type I-type II keratin heterodimers and the vimentin homodimer are highlighted in pink.

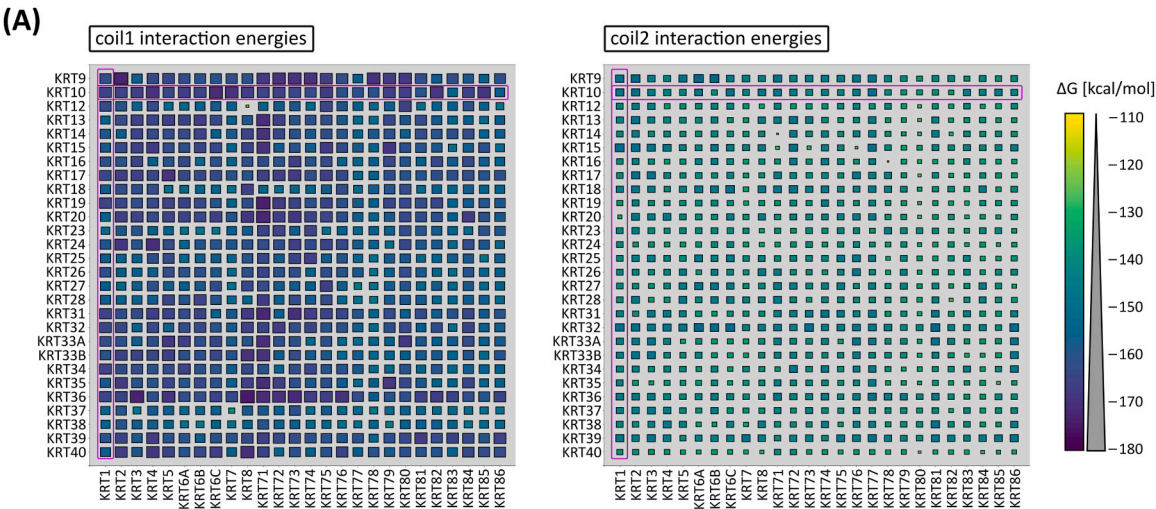


**Fig. 3.** Overview of interaction energies of coil 1 and coil 2 of all putative keratin heterodimers. (A) Heatmap of calculated interaction energies for all modelled keratin heterodimers for coil 1 and coil 2. Interaction energies for both combined (total) can be found in Fig. S3B. The ipTM values for these models ranged between 0.5 and 0.6. Heterodimers involving KRT1 and KRT10 are highlighted in pink.

The distribution of interaction energies furthermore showed for almost all combinations that coil 1 has a lower energy level compared to coil 2 within the same pair. Within coil 1, coil 1B exhibited lower interaction energies than coil 1 A (Table S1). This suggests that the interaction of keratin heterodimers may be predominantly driven or

stabilised by coil 1, specifically coil 1B, with coil 2 playing a lesser role (Fig. 3A, Table S1).

As expected, well-known canonical pairings such as KRT1-KRT10 (total  $\Delta G = -312$  kcal/mol), KRT5-KRT14 (total  $\Delta G = -301$  kcal/mol), KRT6A-KRT16 (total  $\Delta G = -306$  kcal/mol), KRT6A-KRT17 (total

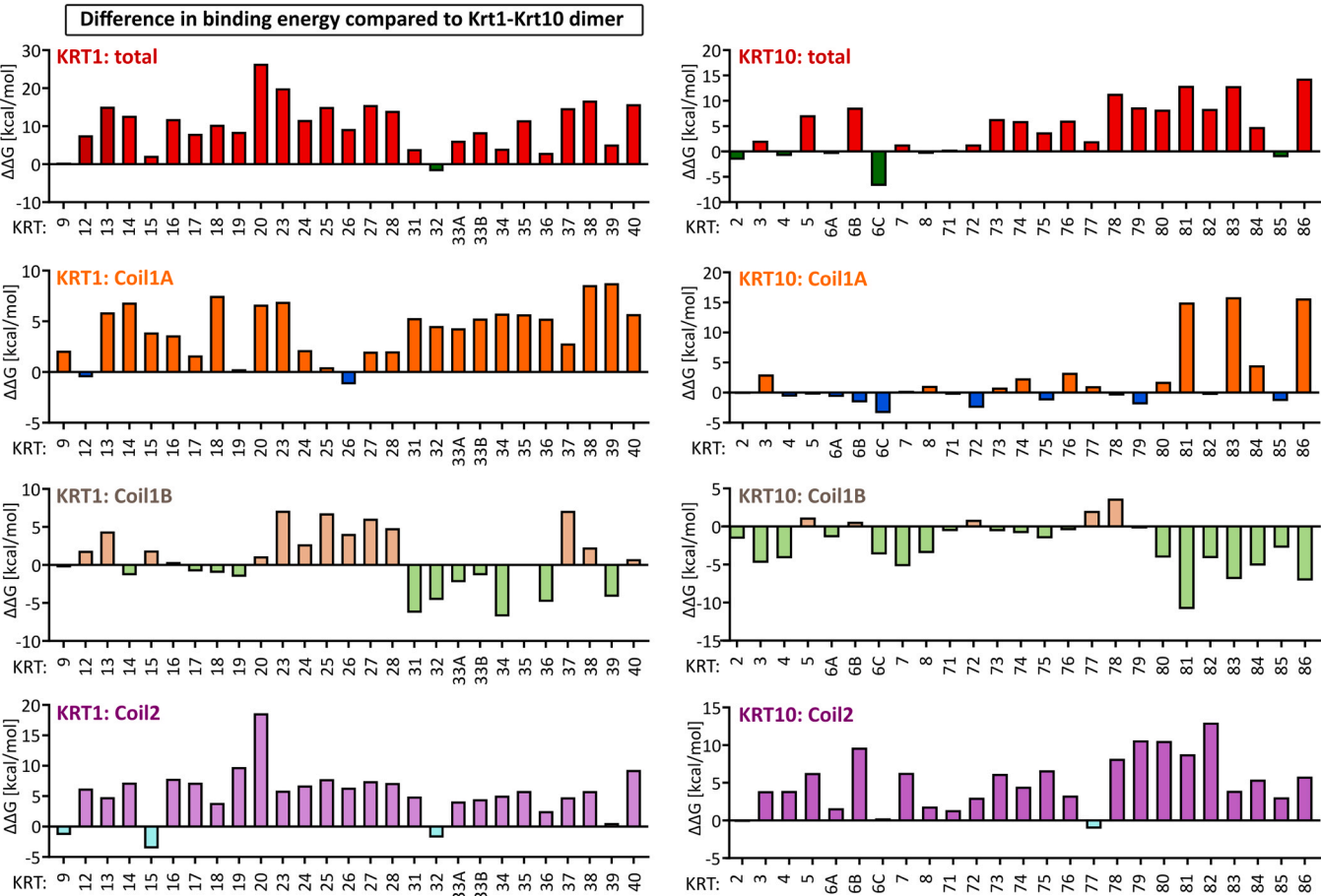


**Fig. 4.** Change in interaction energies of KRT1-KRT10 depending on heterodimer composition. Comparison of the change in interaction energy at 150 mM ionic strength when the heterodimer composition is varied, broken down into the total interaction energy and the contributions from coil 1 A, coil 1 B and coil 2. Results are shown for KRT1 and KRT10.

$\Delta G = -305$  kcal/mol) and KRT8-KRT18 (total  $\Delta G = -312.08$  kcal/mol) show more favourable interaction energies than other combinations (Fig. 3A, Fig. S3B, Table S1). Interestingly, some alternative pairings involving these keratins appear to be equally or occasionally more energetically favourable.

These results provide a comprehensive overview of possible energetically favourable type I-type II heterodimer pairings and thus a robust framework for further comparative analyses.

### 3.4. Analysis of interaction energies predicts a low number of alternative pairings for KRT1 and KRT10

KRT1 and KRT10 are the keratins expressed predominantly, but not exclusively, in the suprabasal layers of the epidermis (Ho et al., 2022; Wiedemann et al., 2023). They form a critical heterodimer that supports the skin's mechanical resilience and barrier function, and mutations in these genes are associated with conditions such as epidermolytic ichthyosis.

To compare this heterodimer with other possible type I or type II combinations, we normalised the calculated interaction energy of the KRT1-KRT10 dimer to zero and then calculated the differences in the total interaction energies when one component of the KRT1-KRT10 dimer is replaced by another keratin of the same type (Fig. 4). We also determined the contributions of each coil region. Since all AlphaFold2 models of the keratin dimer pairs clearly delineate the boundary between coil 1 A and coil 1B, we were also able to distinguish these subregions (Fig. 1B, Fig. 4).

Overall, the change in total interaction energy is mostly positive (e.

g., for KRT13, KRT14 or KRT20) or shows little difference (e.g., for KRT9 or KRT32) when KRT1 is paired with other type I keratins in direct comparison to the KRT1-KRT10 dimer. A positive energy change indicates a less favoured interaction, confirming that the KRT1-KRT10 pairing is most favoured. This trend seems to be mainly influenced by the coil 1 A region and to lesser extent also by coil 2, whereas the energy differences in the coil 1 B subregion are more variable, with some combinations even showing negative energy changes, indicating a more favourable interaction for this sub-region (Fig. 4).

Similarly, when KRT10 is paired with other type II keratins, many combinations also show higher energies, suggesting a less favourable interaction, although some show only marginal changes. Notably, the KRT6C-KRT10 combination appears to be more favourable than KRT1-KRT10. When KRT10 is combined with different type II keratins, the contributions of coil 1 A, coil 1 B and coil 2 vary markedly in their effect on the change in total interaction energy.

In summary, the comparison indicated that the KRT1-KRT10 heterodimer is one of the most favoured combination among those containing KRT1 or KRT10, although other similarly stable and favoured pairings are possible.

### 3.5. Interaction energy analysis predicts many alternative pairings for KRT5 and KRT14

We then investigated alternative dimer partners for the KRT5-KRT14 complex, which is predominantly expressed in the proliferative basal layer of stratified epithelia. To systematically compare interaction dynamics, we generated an overview of interaction differences for

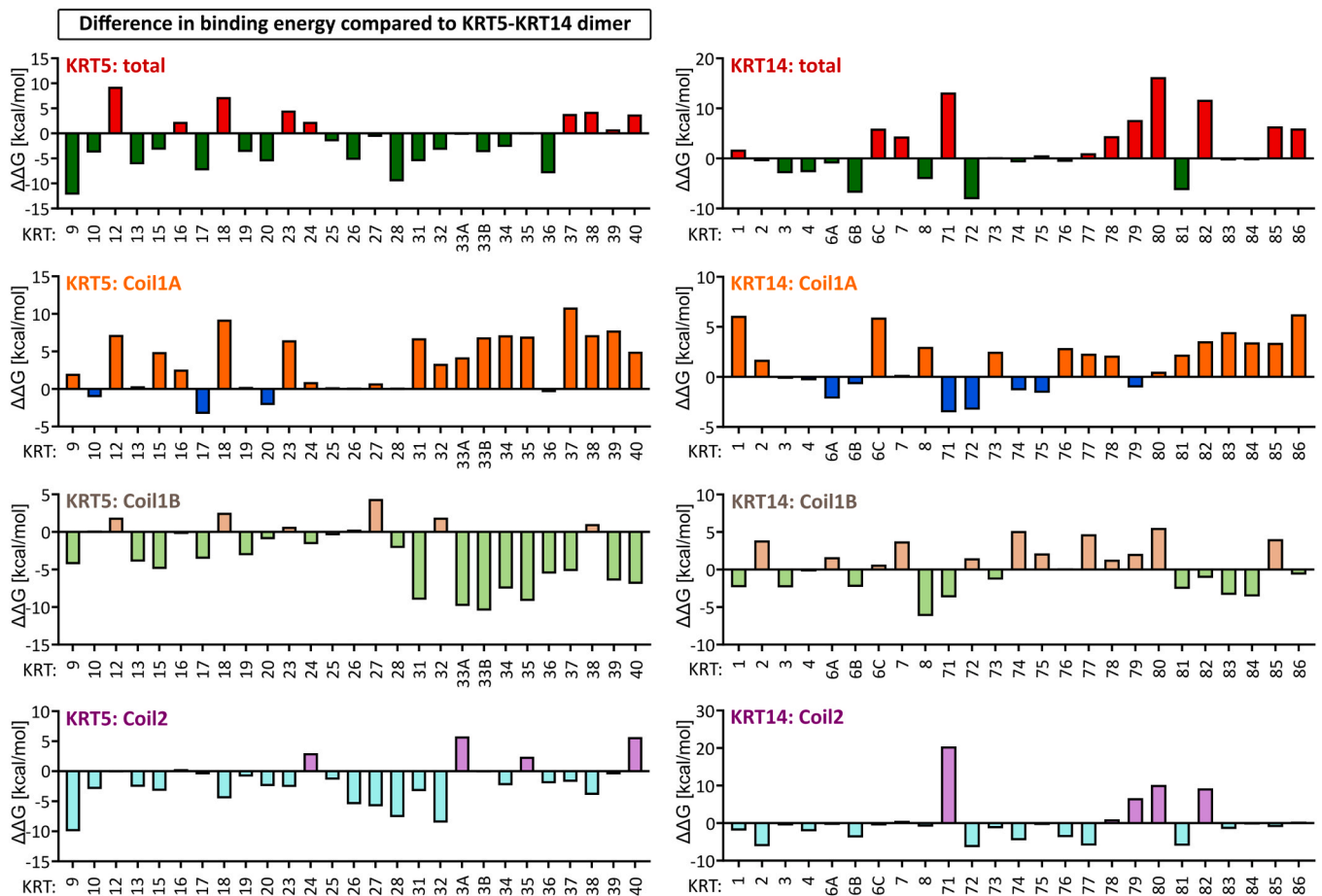


**Fig. 5.** Change in interaction energies of KRT5-KRT14 depending on heterodimer composition. Comparison of the change in interaction energy at 150 mM ionic strength when the heterodimer composition is varied, broken down into the total interaction energy and the contributions from coil 1 A, coil 1 B and coil 2. Results are shown for KRT5 and KRT14.



different alternative pairings, as done for KRT1-KRT10. In contrast to KRT1-KRT10 (Fig. 4), many alternative pairings - whether KRT5 with other type I keratins or KRT14 with other type II keratins - showed more negative interaction energies (Fig. 5). This suggests that alternative pairings, such as KRT5-KRT9 or KRT6B-KRT14, may be more energetically favourable and potentially more stable. Notably, our analysis indicated that the coil 1 B and coil 2 domains exert the greatest influence on the energetic preference of these interactions.

### 3.6. Interaction pair analysis predicts alternative pairings of KRT6 isoforms

Next, we compared KRT6 with its canonical partner KRT16. KRT6 has three defined isoforms—KRT6A, KRT6B, and KRT6C—which differ only by 5 residues in the rod domain (Fig. 6A). Although there are no experimentally solved structures for these dimers, the overall conformation of the KRT6-KRT16 dimers (both coil 1 and coil 2 domains) are similar to those of other keratin dimers (Fig. 1B, D; Fig. 6A). We evaluated several heterodimer combinations using KRT6A-KRT16 as a reference (normalised to zero). Interestingly, most alternative pairings, including those with KRT6B and KRT6C, exhibited less favourable interaction energies, largely due to differences in the coil 1 A region.

We also analysed the KRT6-KRT17 heterodimer, again using KRT6A-KRT17 as a baseline. In this case, all KRT6 isoforms interacted comparably well with KRT17. In contrast, KRT2 and KRT3 appeared to be better partners for KRT17, mainly due to more favourable interactions in coil 1 B and coil 2.

Finally, we examined the KRT6-KRT9 heterodimer, as this combination appears to be generally favoured (Fig. S3B). Here, KRT6A-KRT9 is the most favourable pairing, with coil2 playing a major role, except for the KRT2-KRT9 combination, where the improved interaction is driven by both coil 1 A and coil 1 B.

### 3.7. Spatial transcriptomics in skin show co-expression of keratin dimers

The predictions of alternative keratin heterodimers are only biologically relevant if both keratins are produced in the same cells. Previous studies have shown that alternative keratin pairs are co-expressed in a tissue-specific manner (Ho et al., 2022; Li et al., 2024), but a precise spatial analysis is lacking. To address this, we analysed standardised expression data from the Spatial Transcript Omics DataBase (STOmics DB) (Xu et al., 2024), focusing on skin tissues and their pathological conditions.

As observed before, in healthy skin, keratinocytes show high levels of expression of KRT1, KRT5, KRT10 and KRT14 (Fig. 6C) (Ho et al., 2022). In conditions such as cutaneous squamous cell carcinoma and atopic dermatitis, the expression of these keratins is moderately increased. Noteworthy, KRT6A, KRT6B, KRT6C, KRT16 and KRT17 have very low overall average expression in healthy tissue but are drastically elevated under these pathological conditions making alternative keratin heterodimers with KRT1, KRT5, KRT10 and KRT14 possible (Fig. 4; Fig. 5; Fig. 6B,C).

Overall, single cell spatial transcriptomics unveils fundamental changes in keratin co-expression in the epidermis of healthy and pathological skin.

### 3.8. Mutations associated with epidermolysis bullosa simplex impact the stability of the KRT5-KRT14 heterodimer

To investigate the structural consequences of disease-causing mutations on keratin dimerisation, we used our structural model of the KRT5-KRT14 heterodimer to analyse a set of known pathogenic variants associated with epidermolysis bullosa simplex (EBS) (Fig. 7A). This disease is characterised by skin fragility due to compromised keratin filament assembly and is typically caused by single-point mutations in either KRT5 or KRT14. Using the FoldX5 algorithm, we calculated the

effects of eight such mutations on overall dimer stability, and on dimer interaction energy.

As expected, most of the tested mutations resulted in the destabilisation of the KRT5-KRT14 heterodimer, as evidenced by impaired structural integrity within the entire dimer or in the interaction interface (Fig. 7B). However, depending on their location within the coiled-coil domain, the degree to which these mutations seem to impair heterodimer formation varied considerably.

The KRT14\_R211P and KRT5\_R265P mutations, which are located within the central region of coil 1B, had the most substantial effect on the stability of the heterodimer and the interaction energy (Fig. 7B). These notable changes are likely due to the direct disruption of core inter-helical interactions that are essential for dimer formation. This is consistent with the well-known structural effects of proline substitutions, which introduce kinks into the secondary structure, thereby disrupting its integrity. By contrast, mutations near helix boundaries (KRT14\_R125C, KRT5\_N176S, KRT14\_R417P and KRT5\_R471C) caused moderate reductions in dimer stability.

Interestingly, the two most terminal mutations, KRT5\_R165S and KRT5\_E477K, had a minimal or even slightly positive effect on stability (Fig. 7B), suggesting that their pathogenicity may not arise from disruption of the initial dimerisation process itself, but rather from other possible effects such as impaired higher-order assembly (e.g., tetramer formation and filament bundling) or reduced keratin IF turnover.

Overall, these findings demonstrate the potential of using AlphaFold Multimer models to analyse how clinically relevant mutations may affect the stability of keratin dimer structures, exemplified by KRT5-KRT14 mutations in EBS.

## 4. Discussion

Keratins are essential structural proteins that form the IF network of epithelial cells, providing mechanical stability and resilience. Because of their critical role, defects in keratin filament assembly have been implicated in several human diseases. However, the diversity of keratin polypeptides makes it difficult to investigate all possible interactions using conventional experimental techniques. Our study addressed this challenge by using a high-throughput in silico approach, integrating AlphaFold2 multimer modelling with VoroIF-GNN interface quality assessment and FoldX energy calculations, to systematically map the interaction landscape of keratin rod domains. Our modular segmentation of the coiled-coil domains, along with the exclusion of the disordered head and tail regions, mimicked the fragment-based experimental approach historically used to overcome the unique properties of IFs including insolubility and heterogeneity of keratin IF polymerisation (Chernyatina et al., 2016; Strelkov et al., 2001). Modelling each rod segment in isolation using AlphaFold Multimer improved the scoring and confidence of the IF dimer predictions. The similarity between the experimental and computational approaches highlights a noteworthy principle: breaking down these challenging polymers into manageable components seems to be essential for gaining insight into their molecular architecture. Therefore, our study provides a comprehensive interaction map of the full spectrum of keratin heterodimers and offers guidance for rigorous model evaluation. We demonstrated how AlphaFold2's native confidence scores, which are moderate at best for fragmentary rod domains and poor for full-length constructs, can be supplemented with interface-quality assessments and energy evaluations.

Our analysis confirmed that canonical heterodimer pairings (e.g., KRT1-KRT10, KRT5-KRT14, KRT6-KRT16 and KRT6-KRT17) consistently exhibit more favourable interaction energies compared to homodimers, reinforcing the notion that the initial step of keratin filament assembly is primarily driven by heterodimerisation. Notably, the coil 1 region, particularly coil 1 B (Table S1), appears to be the main contributor to these interactions, while coil 2 plays a lesser role. The preferential stabilisation of keratin dimers by coil 1 B in our keratin



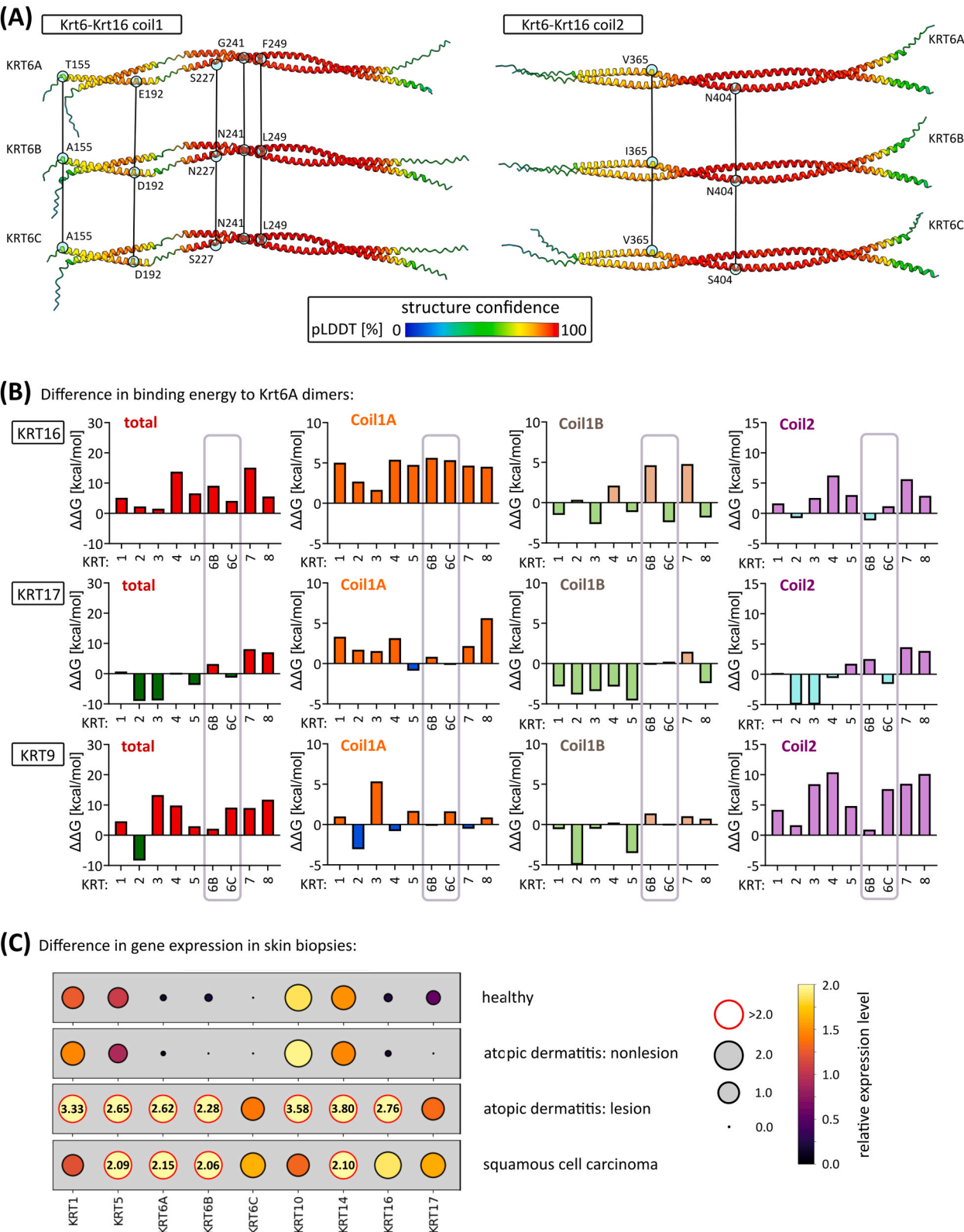


**Fig. 6.** Comparison of KRT6A/KRT6B/KRT6C-KRT16 heterodimerisation and mRNA expression. (A) Heterodimer structures are shown as cartoon representation. The best-ranked AFM models (by ipTM) of the coil 1 and coil 2 regions of the indicated KRT6-KRT16 dimers are coloured by pLDDT scores. Residue positions that differ between KRT6A, KRT6B and KRT6C are labelled. (B) Comparison of the change in interaction energy at 150 mM ionic strength when the KRT6A-KRT16, KRT6A-KRT17 or KRT6A-KRT9 heterodimer composition is varied, broken down into the total interaction energy and the contributions from coil 1 A, coil 1B and coil 2. Dimer composition with KRT6B and KRT6C are highlighted. (C) Spatial transcriptomics data from STomicsDB were used to assess average keratin expression in healthy skin as well as in atopic dermatitis (GSE197023) and cutaneous squamous cell carcinoma (GSE144239).

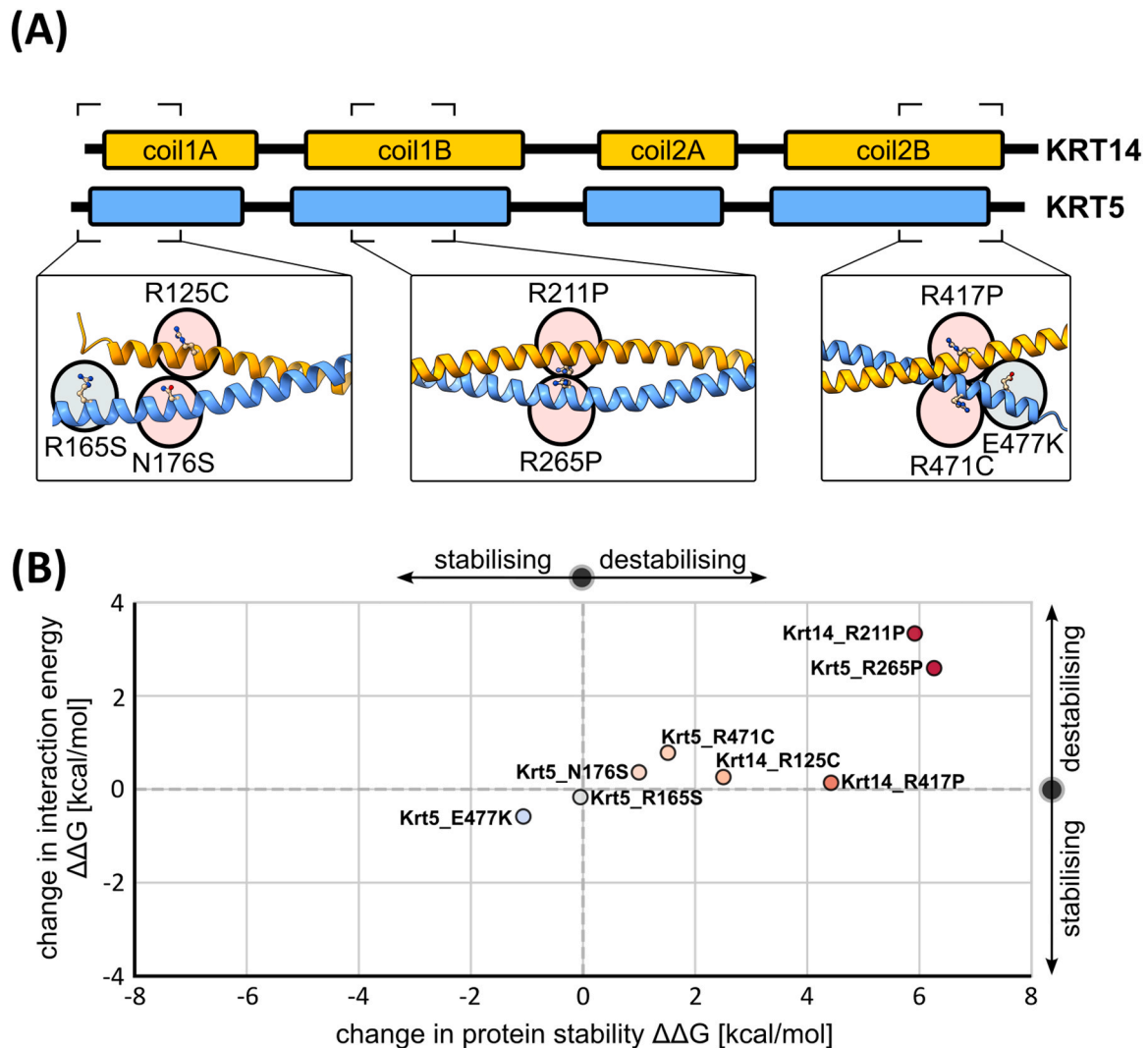


**Fig. 7.** Effects of pathogenic KRT5-KRT14 mutations on stability and dimerisation. (A) The positions of single-point mutations in KRT5-KRT14 that cause epidermolysis bullosa simplex are depicted. (B) FoldX5-calculated changes in overall protein stability and dimer coherence of eight clinically relevant KRT5-KRT14 point mutations associated with epidermolysis bullosa simplex. Positive values indicate destabilisation or weakened binding, while negative values indicate stabilisation.

heterodimers is consistent with earlier findings (Eldirany et al., 2019), which demonstrated that coil 1 B contains structural motifs that stabilise and drive tetramer assembly. Our observation of lower interaction energies for coil 1 B at the dimer stage indicates its importance in heterodimer assembly. Therefore, the intrinsic propensity of coil 1 B to promote dimeric as well as tetrameric interfaces may provide a key molecular basis for the formation of IF assemblies.

Validation against experimentally resolved structures of the vimentin homodimer, KRT1-KRT10 and KRT5-KRT14 further confirmed the accuracy of our models, allowing us to confidently extend our analysis to a wider range of canonical and non-canonical keratin pairs.

Importantly, our results demonstrated that some alternative pairings - such as KRT5-KRT9 and KRT6B-KRT14 - may be as favourable or even more favourable than the canonical combinations. Expression data at the tissue-level (Ho et al., 2022) and spatial transcriptomics (Fig. 6C) suggest that non-canonical interactions may contribute to tissue-specific adaptations, providing an additional layer of regulation during physiological processes or in pathological conditions. Thus, the transition between different epithelial states may be supported by alternative keratin pairing ensuring not only network maintenance but also adaptation to changing functional requirements. The transition from the KRT5-KRT14-positive basal to the KRT1-KRT10-positive suprabasal

compartment in the epidermis reflects such a situation where highly proliferating cells become postmitotic. This change is accompanied by fundamental changes in cell shape, cytoplasmic viscoelasticity and adhesion. Moreover, local differences in epidermal specialisation are supported by additional keratin pairings as is the case in the palmar and plantar epidermis producing KRT9 or wounded epidermis producing KRTs 6, 16 and 17 (Ho et al., 2022) (Fig. 6C). Alternative heterodimerisation may be crucial to remodel filaments through lateral subunit exchange avoiding filament breakdown and re-formation. The ability to computationally predict and rank keratin filer interactions not only streamlines the identification of new pairings but also informs on the design of targeted mutagenesis and biochemical assays for experimental validation.

Structural models of keratin heterodimers provide a powerful new perspective on the molecular basis of keratinopathies. In silico approaches can help to distinguish variants that impair initial dimer formation from those that impair other aspects such as filament assembly or IF turnover. This is achieved by mapping how individual mutations alter helix stability and inter-chain interactions, as demonstrated with pathological KRT5-KRT14 mutations. This mechanistic insight provides an initial classification of potential molecular effects of mutations, allowing for a more selective hypothesis-driven experimental analysis.

Ultimately, rapid computational screening of novel or rare keratin variants could prioritise the most likely pathogenic ones, supporting diagnosis and focusing laboratory validation on the mutations with the putatively highest relevance.

Strikingly, we found that vimentin homodimers appear to be less favourable than heterodimers involving vimentin and type I keratins. Cells that co-express vimentin and type I keratins occur, e.g. in epithelial-mesenchymal transition (EMT) states during tissue repair and in carcinogenesis (Kuburich et al., 2024; Velez-delValle et al., 2016). In these hybrid cells, vimentin has been shown to interact directly with keratins. This interaction relies on the conserved YRKLEGE motif in the vimentin 2B domain (Velez-delValle et al., 2016). In vitro studies also confirm that vimentin and keratin monomers can form mixed coiled-coil heterodimers and even heterotetramers (Nunes Vicente et al., 2022; Steinert et al., 1993; Velez-delValle et al., 2016). However, these hybrid VIM-KRT complexes remain soluble and do not assemble into normal higher-order filaments. Furthermore, VIM-KRT dimers inhibit the assembly of both vimentin and keratin filaments (Kuburich et al., 2024; Steinert et al., 1993; Velez-delValle et al., 2016). Taken together, these data suggest that the predicted more favourable VIM-KRT dimer compared to a vimentin homodimer reflects a high binding affinity in vivo, but one that destabilises keratin filaments. Thus, increased levels of vimentin could sequester type I keratins away from their normal type II partners, thereby preventing normal type I-II filament formation. This 'poisoning' of the keratin network may facilitate epithelial-mesenchymal transition (EMT) by breaking down the rigid epithelial IF scaffold (Kuburich et al., 2024; Steinert et al., 1993; Velez-delValle et al., 2016).

Furthermore, our findings also highlight high-confidence heterodimer predictions between  $\beta$ -actin and the coil 2 region of various keratins and vimentin. Our predictions are consistent with previous observations indicating that keratin filament dynamics are closely linked to the organisation of actin. In particular, the inward translocation of keratin precursors has been shown to depend on intact actin filaments (Kölsch et al., 2009), and studies in *Xenopus* oocytes have demonstrated that the polarity of the keratin network is maintained by an F-actin-dependent architecture (Gard et al., 1997). Our predictions are noteworthy because actin-IF crosstalk has traditionally been believed to occur via adaptor proteins, such as plectin (Outla et al., 2025). While our results suggest the existence of a direct actin-keratin interface with broad implications for cytoskeletal organisation and mechanics, future biochemical and structural studies are essential to experimentally validate these interactions and clarify their role in cytoskeletal architecture.

Despite these promising findings, our approach has limitations. We have only focused on the structured rod domains and dimer formation, as the full keratin proteins with the flexible head and tail regions, filament assembly and dynamic behaviour of keratins, including post-translational modifications and higher order multimers, remain difficult to capture computationally. Future studies incorporating molecular dynamics simulations and targeted experiments will be essential to fully elucidate the kinetic and structural nuances of both canonical and alternative keratin pairings in the broader context of filament assembly.

In summary, our computational framework provides new insights into the energy landscapes governing keratin dimerisation, thereby enhancing our understanding of IF assembly. This comprehensive overview lays the groundwork for future experimental investigations and could ultimately advance the understanding of keratin-related disorders and thus inform novel therapeutic strategies.

## Funding

The research was supported by the German Research Council (363055819/GRK2415) to N.S. and R.E.L. and (556125570) to S.D., as well as by the German Federal Ministry of Education and Research (01KD24235) to S.D.

## CRediT authorship contribution statement

**Nicole Schwarz:** Writing – review & editing, Validation, Formal analysis, Conceptualization. **Rudolf E Leube:** Writing – review & editing, Validation, Formal analysis, Conceptualization. **Stefan Dusterhöft:** Writing – review & editing, Writing – original draft, Validation, Methodology, Formal analysis, Conceptualization.

## Declaration of Competing Interest

The authors declare that they have no known competing financial interests or personal relationships that could have appeared to influence the work reported in this paper.

## Appendix A. Supporting information

Supplementary data associated with this article can be found in the online version at doi:10.1016/j.ejcb.2025.151513.

## Data availability

Data will be made available on request.

## References

- Aziz, A., Hess, J.F., Budamagunta, M.S., Voss, J.C., Kuzin, A.P., Huang, Y.J., Xiao, R., Montellione, G.T., FitzGerald, P.G., Hunt, J.F., 2012. The structure of vimentin linker 1 and rod 1B domains characterized by site-directed spin-labeling electron paramagnetic resonance (SDSL-EPR) and X-ray crystallography. *J. Biol. Chem.* 287, 28349–28361.
- Bunick, C.G., Milstone, L.M., 2017. The X-Ray crystal structure of the keratin 1-Keratin 10 helix 2B heterodimer reveals molecular surface properties and biochemical insights into human skin disease. *J. Invest. Dermatol.* 137, 142–150.
- Chernyatina, A.A., Hess, J.F., Guzenko, D., Voss, J.C., Strelkov, S.V., 2016. How to study intermediate filaments in atomic detail. *Methods Enzym.* 568, 3–33.
- Cohen, E., Johnson, C., Redmond, C.J., Nair, R.R., Coulombe, P.A., 2022. Revisiting the significance of keratin expression in complex epithelia. *J. Cell Sci.* 135.
- Cohen, E., Johnson, C.N., Wasikowski, R., Billi, A.C., Tsoi, L.C., Kahlenberg, J.M., Gudjonsson, J.E., Coulombe, P.A., 2024. Significance of stress keratin expression in normal and diseased epithelia. *iScience* 27, 108805.
- Eldirany, S.A., Ho, M., Hinbest, A.J., Lomakin, I.B., Bunick, C.G., 2019. Human keratin 1/10-1B tetramer structures reveal a knob-pocket mechanism in intermediate filament assembly. *EMBO J.* 38.
- Evans, R., O'Neill, M., Pritzel, A., Antropova, N., Senior, A., Green, T., Židek, A., Bates, R., Blackwell, S., Yim, J., Ronneberger, O., Bodenstein, S., Zielinski, M., Bridgland, A., Potapenko, A., Cowie, A., Tunyasuvunakool, K., Jain, R., Clancy, E., Kohli, P., Jumper, J., Hassabis, D., 2021. Protein complex prediction with AlphaFold-Multimer. *bioRxiv*, 2021.2010.2004.463034.
- Gard, D.L., Cha, B.J., King, E., 1997. The organization and animal-vegetal asymmetry of cytokeratin filaments in stage VI *xenopus* oocytes is dependent upon F-actin and microtubules. *Dev. Biol.* 184, 95–114.
- Hatzfeld, M., Franke, W.W., 1985. Pair formation and promiscuity of cytokeratins: formation in vitro of heterotypic complexes and intermediate-sized filaments by homologous and heterologous recombinations of purified polypeptides. *J. Cell Biol.* 101, 1826–1841.
- Ho, M., Thompson, B., Fisk, J.N., Nebert, D.W., Bruford, E.A., Vasiliou, V., Bunick, C.G., 2022. Update of the keratin gene family: evolution, tissue-specific expression patterns, and relevance to clinical disorders. *Hum. Genom.* 16, 1.
- Ji, A.L., Rubin, A.J., Thrane, K., Jiang, S., Reynolds, D.L., Meyers, R.M., Guo, M.G., George, B.M., Mollbrink, A., Bergenstrahle, J., Larsson, L., Bai, Y., Zhu, B., Bhaduri, A., Meyers, J.M., Rovira-Clave, X., Hollmig, S.T., Aasi, S.Z., Nolan, G.P., Lundberg, J., Khavari, P.A., 2020. Multimodal analysis of composition and spatial architecture in human squamous cell carcinoma. *Cell* 182, 497–514 e422.
- Jumper, J., Evans, R., Pritzel, A., Green, T., Figurnov, M., Ronneberger, O., Tunyasuvunakool, K., Bates, R., Židek, A., Potapenko, A., Bridgland, A., Meyer, C., Kohli, S.A.A., Ballard, A.J., Cowie, A., Romera-Paredes, B., Nikolov, S., Jain, R., Adler, J., Back, T., Petersen, S., Reiman, D., Clancy, E., Zielinski, M., Steinegger, M., Pacholska, M., Berghammer, T., Bodenstein, S., Silver, D., Vinyals, O., Senior, A.W., Kavukcuoglu, K., Kohli, P., Hassabis, D., 2021. Highly accurate protein structure prediction with AlphaFold. *Nature* 596, 583–589.
- Kölsch, A., Windoffer, R., Leube, R.E., 2009. Actin-dependent dynamics of keratin filament precursors. *Cell Motil. Cytoskelet.* 66, 976–985.
- Kuburich, N.A., Kiselka, J.M., den Hollander, P., Karam, A.A., Mani, S.A., 2024. The cancer chimera: impact of vimentin and cytokeratin Co-Expression in hybrid Epithelial/Mesenchymal cancer cells on tumor plasticity and metastasis. *Cancers* 16.
- Lee, C.H., Kim, M.S., Chung, B.M., Leahy, D.J., Coulombe, P.A., 2012. Structural basis for heteromeric assembly and perinuclear organization of keratin filaments. *Nat. Struct. Mol. Biol.* 19, 707–715.

- Lee, C.H., Kim, M.S., Li, S., Leahy, D.J., Coulombe, P.A., 2020. Structure-Function analyses of a keratin heterotypic complex identify specific keratin regions involved in intermediate filament assembly. *Structure* 28, 355–362 e354.
- Li, G., Guo, J., Mou, Y., Luo, Q., Wang, X., Xue, W., Hou, T., Zeng, T., Yang, Y., 2024. Keratin gene signature expression drives epithelial-mesenchymal transition through enhanced TGF-beta signaling pathway activation and correlates with adverse prognosis in lung adenocarcinoma. *Heliyon* 10, e24549.
- Lomakin, I.B., Hinbest, A.J., Ho, M., Eldirany, S.A., Bunick, C.G., 2020. Crystal structure of keratin 1/10(C401A) 2B heterodimer demonstrates a proclivity for the C-Terminus of helix 2B to form higher order molecular contacts. *Yale J. Biol. Med.* 93, 3–17.
- Madaj, R., Martinez-Goicoetxea, M., Kaminski, K., Ludwiczak, J., Dunin-Horkawicz, S., 2025. Applicability of AlphaFold2 in the modeling of dimeric, trimeric, and tetrameric coiled-coil domains. *Protein Sci.* 34, e5244.
- Mirdita, M., Schutze, K., Moriawaki, Y., Heo, L., Ovchinnikov, S., Steinegger, M., 2022. ColabFold: making protein folding accessible to all. *Nat. Methods* 19, 679–682.
- Moll, R., Divo, M., Langbein, L., 2008. The human keratins: biology and pathology. *Histochem Cell Biol.* 129, 705–733.
- Nicolet, S., Herrmann, H., Aebi, U., Strelkov, S.V., 2010. Atomic structure of vimentin coil 2. *J. Struct. Biol.* 170, 369–376.
- Nunes Vicente, F., Lelek, M., Tinevez, J.Y., Tran, Q.D., Pehau-Arnaudet, G., Zimmer, C., Etienne-Manneville, S., Giannone, G., Leduc, C., 2022. Molecular organization and mechanics of single vimentin filaments revealed by super-resolution imaging. *Sci. Adv.* 8, eabm2696.
- Olechnovic, K., Venclovas, C., 2023. VoroIF-GNN: voronoi tessellation-derived protein-protein interface assessment using a graph neural network. *Proteins* 91, 1879–1888.
- Outla, Z., Oyman-Eyrimelmez, G., Korelova, K., Prechova, M., Frick, L., Sarnova, L., Bisht, P., Novotna, P., Kosla, J., Bortel, P., Borutski, Y., Bileck, A., Gerner, C., Rahbari, M., Rahbari, N., Birgin, E., Kvasnicova, B., Galisova, A., Sulkova, K., Bauer, A., Jobe, N., Tolde, O., Sticova, E., Rösel, D., O'Connor, T., Otahal, M., Jirak, D., Heikenwälder, M., Wiche, G., Meier-Menches, S.M., Gregor, M., 2025. Plectin-mediated cytoskeletal crosstalk as a target for inhibition of hepatocellular carcinoma growth and metastasis. *eLife* 13.
- Pang, A.H., Obiero, J.M., Kulczyk, A.W., Sviripa, V.M., Tsodikov, O.V., 2018. A crystal structure of coil 1B of vimentin in the filamentous form provides a model of a high-order assembly of a vimentin filament. *FEBS J.* 285, 2888–2899.
- Pettersen, E.F., Goddard, T.D., Huang, C.C., Meng, E.C., Couch, G.S., Croll, T.I., Morris, J. H., Ferrin, T.E., 2021. UCSF ChimeraX: structure visualization for researchers, educators, and developers. *Protein Sci.* 30, 70–82.
- Redmond, C.J., Coulombe, P.A., 2021. Intermediate filaments as effectors of differentiation. *Curr. Opin. Cell Biol.* 68, 155–162.
- Schwarz, N., Leube, R.E., 2023. Plasticity of cytoplasmic intermediate filament architecture determines cellular functions. *Curr. Opin. Cell Biol.* 85, 102270.
- Steinert, P.M., Marekov, L.N., Parry, D.A., 1993. Diversity of intermediate filament structure. Evidence that the alignment of coiled-coil molecules in vimentin is different from that in keratin intermediate filaments. *J. Biol. Chem.* 268, 24916–24925.
- Strelkov, S.V., Herrmann, H., Geisler, N., Lustig, A., Ivaninskii, S., Zimbelmann, R., Burkhard, P., Aebi, U., 2001. Divide-and-conquer crystallographic approach towards an atomic structure of intermediate filaments. *J. Mol. Biol.* 306, 773–781.
- Strelkov, S.V., Herrmann, H., Geisler, N., Wedig, T., Zimbelmann, R., Aebi, U., Burkhard, P., 2002. Conserved segments 1A and 2B of the intermediate filament dimer: their atomic structures and role in filament assembly. *EMBO J.* 21, 1255–1266.
- Toivola, D.M., Boor, P., Alam, C., Strnad, P., 2015. Keratins in health and disease. *Curr. Opin. Cell Biol.* 32, 73–81.
- UniProt, C., 2024. UniProt: the universal protein knowledgebase in 2025. *Nucleic Acids Res.*
- Van Durme, J., Delgado, J., Stricher, F., Serrano, L., Schymkowitz, J., Rousseau, F., 2011. A graphical interface for the FoldX forcefield. *Bioinformatics* 27, 1711–1712.
- Varadi, M., Anyango, S., Deshpande, M., Nair, S., Natassia, C., Yordanova, G., Yuan, D., Stroe, O., Wood, G., Laydon, A., Zidek, A., Green, T., Tunyasuvunakool, K., Petersen, S., Jumper, J., Clancy, E., Green, R., Vora, A., Lutfi, M., Figurnov, M., Cowie, A., Hobbs, N., Kohli, P., Kleywegt, G., Birney, E., Hassabis, D., Velankar, S., 2022. AlphaFold protein structure database: massively expanding the structural coverage of protein-sequence space with high-accuracy models. *Nucleic Acids Res* 50, D439–D444.
- Velez-delValle, C., Marsch-Moreno, M., Castro-Munozledo, F., Galvan-Mendoza, L.J., Kuri-Harcuch, W., 2016. Epithelial cell migration requires the interaction between the vimentin and keratin intermediate filaments. *Sci. Rep.* 6, 24389.
- Wiedemann, J., Billi, A.C., Bocci, F., Kashgari, G., Xing, E., Tsoi, L.C., Meller, L., Swindell, W.R., Wasikowski, R., Xing, X., Ma, F., Gharaee-Kermani, M., Kahlenberg, J.M., Harms, P.W., Maverakis, E., Nie, Q., Gudjonsson, J.E., Andersen, B., 2023. Differential cell composition and split epidermal differentiation in human palm, sole, and hip skin. *Cell Rep.* 42, 111994.
- Wu, H., Shen, Y., Sivagurunathan, S., Weber, M.S., Adam, S.A., Shin, J.H., Fredberg, J.J., Medalia, O., Goldman, R., Weitz, D.A., 2022. Vimentin intermediate filaments and filamentous actin form unexpected interpenetrating networks that redefine the cell cortex. *Proc. Natl. Acad. Sci. USA* 119, e2115217119.
- Xu, Z., Wang, W., Yang, T., Li, L., Ma, X., Chen, J., Wang, J., Huang, Y., Gould, J., Lu, H., Du, W., Sahu, S.K., Yang, F., Li, Z., Hu, Q., Hua, C., Hu, S., Liu, Y., Cai, J., You, L., Zhang, Y., Li, Y., Zeng, W., Chen, A., Wang, B., Liu, L., Chen, F., Ma, K., Xu, X., Wei, X., 2024. STOmicsDB: a comprehensive database for spatial transcriptomics data sharing, analysis and visualization. *Nucleic Acids Res* 52, D1053–D1061.
- Yoon, S., Leube, R.E., 2019. Keratin intermediate filaments: intermediaries of epithelial cell migration. *Essays Biochem.* 63, 521–533.
- Zhou, X., Lin, Y., Kato, M., Mori, E., Liszczak, G., Sutherland, L., Sysoev, V.O., Murray, D. T., Tycko, R., McKnight, S.L., 2021. Transiently structured head domains control intermediate filament assembly. *Proc. Natl. Acad. Sci. USA* 118.